Graphical abstract

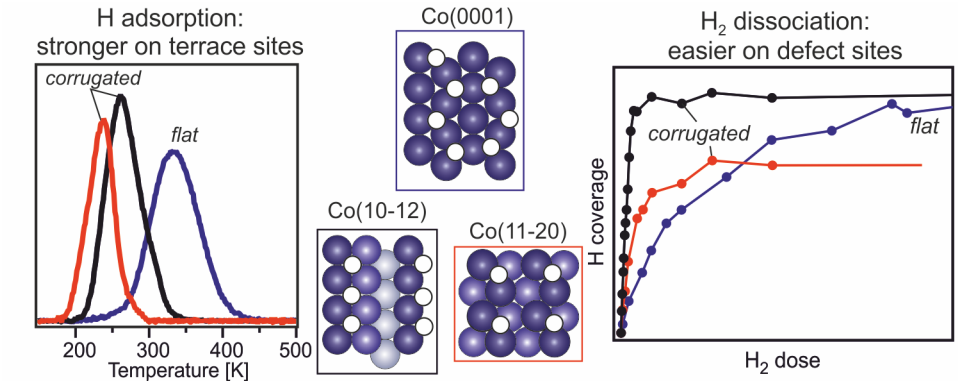

Interaction of hydrogen with flat (0001) and corrugated (11-20) and (10-12) cobalt surfaces: Insights from experiment and theory

C.J. (Kees-Jan) Weststrate[a], Mehdi Mahmoodinia[b], Mari Helene Farstad[b], Ingeborg-Helene Svenum[b,c], Marie D. Strømsheim[b], J.W. (Hans) Niemantsverdriet[a,d], Hilde J. Venvik[b]

[a]SynCat@DIFFER, Syngaschem BV, P.O. Box 6336, 5600 HH Eindhoven, The Netherlands

[b]Department of Chemical Engineering, Norwegian University of Science and Technology (NTNU), 7491, Trondheim, Norway

[c]SINTEF Industry, Postboks 4760 Torgarden, 7465 Trondheim, 7465, Norway

[d]SynCat@Beijing, Synfuels China Technology Co. Ltd., Leyuan South Street II, No. 1, Huairou District, 101407 Beijing, China

Abstract

Cobalt catalysts are used on a commercial scale to produce synthetic fuels via the Fischer-Tropsch synthesis reaction. Adsorbed hydrogen atoms are involved in many of the elementary reaction steps that occur on the catalyst surface. In this study we use a combination of experimental and theoretical methods to gain insight into how the structure of a cobalt surface affects the H_2 dissociation reaction and the adsorption bond strength of the hydrogen atoms produced in this step. A comparison of the open Co(11-20) and (10-12) surfaces with the flat, close packed Co(0001) surface confirms that undercoordinated Co atoms strongly enhance the rate of H_2 dissociation. The lower desorption temperatures found on the more open surfaces indicate that the bond strength of adsorbed hydrogen decreases in the following order: Co(0001)>Co(10-12)>Co(11-20). DFT calculations confirm this trend, showing that hydrogen adsorbs weaker on the more open surfaces for both low and high coverages. In the context of the Fischer-Tropsch synthesis reaction we propose that step and kink sites are important for efficient H_2 dissociation. After dissociation, the higher hydrogen adsorption strength on terrace sites would promote diffusion away from the dissociation site to flat terraces where they can participate in hydrogenation reactions.

Introduction

In the Fischer-Tropsch synthesis reaction, the carbon and oxygen atoms of the CO precursor molecule react with surface hydrogen atoms to form C_xH_y and H_2O. By using a cobalt-based catalyst operated at relatively low temperature, around or below 500 K, the selectivity of this reaction can be tuned to produce long chain aliphatic hydrocarbons. The product, synthetic wax of high purity, can be employed in various ways, one important route being the cracking of the syncrude to kerosene and diesel fractions to produce synthetic fuels of high purity.

The active phase of industrially applied cobalt catalysts consists of metallic nanoparticles with a typical size of around 5-10 nm [1]. One of the elementary reaction steps that occurs on the surface of these particles is the dissociative adsorption of H_2 to produce surface hydrogen atoms, the active species in hydrogenation steps on the surface.

Small metallic nanoparticles expose a heterogeneous surface with a large a variety of active sites. On fcc-cobalt particles flat (111) and (100) facets dominate, with monoatomic steps and kinks as the most common defect sites [2]. For metallic nanoparticles with a hcp bulk structure the close-packed (0001) surface can only be formed on two opposing sides of the particle, whereas the remaining sides expose more open surfaces [3,4] such as the (10-10) and the (10-11) surface. The Co(10-12) and Co(11-20) used in the present study are exposed as well on such particles.

Although the H_2 molecule is one of the reactants in FTS synthesis, there is only a limited number of experimental studies in which the interaction of H_2 with single crystal surfaces of cobalt is discussed. On Co(0001) it has been found that the initial dissociative sticking coefficient of H_2 is not very high, with a value of around 0.01−0.05 [5–8]. The same studies show that the activation energy for desorption is in the order of 90-100 kJ mol^{-1}. Dissociation of H_2 becomes activated on a surface covered with 0.5 ML H_{ad}. As a result, the dissociative

sticking coefficient decreases so much that UHV-type pressures are too low to produce a surface coverage beyond 0.5 ML [5–7,9]. The notion that H_2 dissociation is practically barrierless on an empty surface [10] but becomes increasingly activated when hydrogen atoms are present on the surface is confirmed by experiments performed by Sicot et al. [11]. In their STM study of bilayer cobalt islands on a Cu(111) template they found that dissociative adsorption of H_2 occurs even at 10 K. Dissociation stops when a coverage of 0.25 ML H_{ad} is reached, and instead the adsorption of molecular H_2 is reported to occur alongside the H_{ad}. This implies that H_2 dissociation becomes activated at a coverage of 0.25 ML already, and a temperature of 10 K is too low to overcome this barrier.

Similar to other metal surfaces such as Pt and Ni [12,13], the surface atoms with a low coordination number which are exposed on step and kink sites enhance H_2 dissociation on surfaces of cobalt. On Co(0001), surface defects formed by a sputter treatment at room temperature enhance H_2 dissociation and a dissociative sticking coefficient close to unity is found on a defect-rich surface [5]. Surface defects furthermore allow the population of hydrogen sites associated with a dissociation barrier on the flat surface. In this way an atomic hydrogen coverage beyond 0.5 ML can be reached for a relatively low dose of H_2 on sputter-damaged Co(0001). Taking a somewhat different approach, Sykes and co-workers were able to prepare a (1×1) (1 ML) H_{ad} layer on Cu(111)-supported bilayer Co islands [14,15]. In this case the undercoordinated sites at the edges of the Co island facilitate H_2 dissociation. Beside these studies only the Co(10-10) surface has been studied experimentally [16]. Analysis of the thermal desorption spectra yielded an activation energy for desorption of 80 kJ mol^{-1}, significantly lower than that of the flat surface.

A theoretical approach has been used by a number of groups to investigate how hydrogen atoms and di-hydrogen molecules interact with hcp-Co(0001) [5,9,17,18], various flat and stepped fcc-Co surfaces [5,19–21] or unsupported Co_6 and Co_{13} clusters [22]. In their study

of the dynamics of dissociative H_2 adsorption on Co(0001) Jiang et al. show that the minimum energy pathway for dissociative adsorption is dissociation on/over the top site [17]. For an empty surface a barrier height of 0.04 eV was found, close to the average kinetic energy of H_2 at room temperature so that dissociative adsorption readily occurs on the empty surface under all practical conditions. The adsorption strength of hydrogen atoms was found to depend on the structure of the surface. For the low coverage limit the calculations by Yu et al. and Wang et al. [19,21] indicate the following order of stability: Co(111) >Co(311)>Co(100)>Co(110). The work by both Klinke et al. [9,18] shows that the formation of subsurface hydrogen is endothermic with respect to H_2 (g) on Co(0001), which implies that subsurface hydrogen does not form under realistic conditions.

In the present study we use an experimental approach to study how the structure of the cobalt surface affects dissociative adsorption of the H_2 molecule. Our experiments also provide information about the adsorption strength of hydrogen atoms as a function of surface structure. The experimental work is complemented by an in-depth theoretical investigation in which we explore the adsorption site and adsorption strength of hydrogen atoms adsorbed on three different single crystal surfaces of cobalt. By systematically studying the effect of surface coverage we get insight into how lateral interactions affect the bond strength and determine which adsorption sites are the most preferred at each coverage.

Three different cobalt surfaces were used in this study: Co(0001), Co(10-12) and Co(11-20). The close-packed Co(0001) surface has been studied previously and serves as a reference point[5–7]. The other two surfaces were selected since they expose different types of undercoordinated surface atoms. In addition to this, their structure in the clean state is well-known, as earlier scanning tunnelling microscopy (STM) and low energy electron diffraction (LEED) studies have shown that their structure in the clean state is close to the bulk-terminated structure [23–25].

Materials and methods

Experimental procedures: The experiments were performed in a UHV system equipped with LEED/Auger optics, a sputter gun for sample cleaning and a differentially pumped quadrupole mass spectrometer. The disc-shaped samples were held in place by a U-shaped W support wire in thermal contact with a liquid nitrogen reservoir, allowing a temperature of around ~95 K. Sample heating was achieved by passing a direct current through the support wire. The sample temperature was measured by a K-type thermocouple, spotwelded to the backside of the sample. For both Co(0001) and Co(10-12) a disc-shaped single crystal with a thickness of 2 mm and a diameter of 8 mm was used. The Co(11-20) sample used in this study is disk-shaped, with a thickness of 1.5 mm thick and a diameter of 10 mm. The maximum temperature used in sample preparation and during experiments was kept below 670 K to stay clear from the hcp-fcc phase transition temperature of Co. Hydrogen doses are reported in Langmuir (1 L = 1×10^{-6} Torr·s) and were calculated using an ion gauge sensitivity factor of 0.35 to account for the low sensitivity for H_2.

A typical cleaning cycle consists of sputtering using 0.7-1 kV Ar^+ while the sample is held at 650-670 K, followed by annealing in vacuum at the same temperature. Sample cleanliness was verified by LEED and Auger. During the TPD experiment the sample was positioned 2 mm away from the 5 mm wide opening of the differentially pumped QMS housing to eliminate desorption from other parts of the sample holder from the desorption spectra. In this approach the signal intensity depends on the exact distance between sample and the opening of the MS compartment, making a quantitative comparison of the amount of H_2 desorbed from two different samples complicated. The sample holder design minimizes the desorption from other parts of the sample holder, allowing us to use the pressure rise in the vacuum system during the TPD experiment for quantification. Since two samples can be mounted on the same sample holder it is possible to quickly change from one sample to another. By using

the known saturation value of 0.5 ML on Co(0001) as a reference point [5–7,9] and taking the differences in surface area of the different samples into account we were able to determine the absolute quantity of H_2 desorbing from the (10-12) and (11-20) samples. Since the monolayer definition becomes ambiguous for the open surfaces used here, we instead report hydrogen surface coverages as the number of adsorbate atoms per nm^2.

Computational methods: All quantum chemical calculations reported here were carried out using spin-polarized DFT within the generalized gradient approximation (GGA). The projector-augmented wave (PAW) method [26,27] implemented in the Vienna Ab initio Simulation Package (VASP) [28,29] together with a plane wave basis set with 500 eV energy cut-off were used to describe the interactions between ion cores and valence electrons. The Perdew-Burke-Ernzerhof (PBE) functional [20,30] has been used for the exchange-correlation energy of electrons. The k-point sampling was performed with the Γ-centered Monkhorst-Pack scheme [31], and using a 5×5×1 k-point grid. The partial occupancies for each wavefunction were modelled by the approach proposed by Methfessel-Paxton [32] with a smearing width of 0.1 eV. The lattice parameters of bulk hcp Co were calculated as a=2.48 Å and c=4.04 Å. A magnetic moment of 1.64 μ_B per Co atom was obtained. These values are in good agreement with experimentally obtained values of a=2.51 and c=4.07 Å [33], and a magnetic moment of 1.72 μ_B/atom [34]. A five-layer slab with a vacuum region of about 10 Å between the repeating surfaces was used to model the Co(0001), Co(11–20) and Co(10–12) terminations, which were represented using p(3×3), p(2×1), and p(3×1) surface unit cells, respectively. For structural relaxation calculations, the bottom two layers of atoms were kept fixed at their equilibrium positions, and the remaining layers were allowed to relax until the force components on each atom were less than 0.001 eV/Å. The convergence criterion for electronic self-consistent iteration was set to10^{-6} eV.

The gas-phase H_2 molecule was calculated by placing it inside a simple cubic unit cell with 10 Å sides. The equilibrium bond distance, vibrational frequency and binding energy of the H_2 were calculated as 0.750 Å, 4330 cm^{-1}, and 4.54 eV, which are in fairly good agreement with the experimental value [35] of 0.74 Å, 4395 cm^{-1}, and 4.75 eV, respectively, and almost identical to previous DFT results . For the calculations of adsorbed hydrogen, the H atoms were adsorbed on one side of the Co surface slabs. To avoid artificial dipole effects, a dipole correction to the total energy was applied [36]. Vibrational frequency analyses were performed using the finite-difference method in order to identify the stationary points and also to include the zero-point vibrational correction to the adsorption energies. The zero-point energies (E_{ZPE}) of Co atoms were assumed to be unchanged upon adsorption, while the adsorbed H atoms were allowed to displace in each direction by ±0.015 Å. The adsorption energy (E_{ads}) of hydrogen atom on different adsorption sites of the corresponding surfaces were calculated as:

$$E_{ads} = (E_{slab+nH} + E_{ZPE}) - (E_{slab} + \frac{n}{2}(E_{H2} + E_{ZPE})) \qquad (1)$$

where the E_{slab} , E_{slab+H}, and E_{H2} are total energies of the relaxed clean slabs, slabs with adsorbed H, and an isolated hydrogen molecule, respectively. Negative adsorption energy indicates that adsorption of H on the corresponding adsorption site is favourable. In order to study the effects of H coverage, and to probe the coverage-dependent differential adsorption energy curve, H atoms were sequentially introduced onto the Co surfaces, and the binding energy of the additional H atom was calculated as:

$$\Delta E_{\mathrm{H}} = E(slab + n\mathrm{H}) - E(slab + (n-1)\mathrm{H}) - \frac{1}{2}(E_{\mathrm{H2}}) \qquad (2)$$

Were ΔE_{H} and is the differential adsorption energy. The differential Gibbs free energy of adsorption, ΔG_{ads}, was calculated as:

$$\Delta G_{ads} = \Delta \mathrm{E_H} + \Delta E_{\mathrm{ZPE}} - T\Delta S_{\mathrm{H}} \qquad (3)$$

Where ΔE_{ZPE} is the difference between ZPE of the adsorbed H and H in the gas phase H_2. T is temperature (K), and ΔS_H is the entropy difference between the adsorbed H and gas phase H_2 molecule. Entropy for adsorbed H atoms was derived from the DFT-calculated vibrational frequencies [37], and for the gas phase H_2 molecule it was calculated from Shomate equation, explained here [38], where its related parameters were taken from NIST chemistry webbook. Hydrogen adsorption was performed at 100 K in the experiments and this temperature was therefore used to calculate the Gibbs free energy change.

All possible high-symmetry adsorption sites were investigated for adsorption of H atoms and to study the effect of surface coverage. In order to facilitate comparison with experimental results, the H coverage is expressed as the number of H atoms per nm^2. All illustrations of the optimized geometries were produced using the Visualization for Electronic and Structural Analysis (VESTA) program [39].

Experimental Results

Fig. 1 shows the structure of the three Co surfaces investigated. The LEED patterns of the clean surface indicate a good surface quality of the samples. It should be noted that two possible terminations exist for the Co(10-12) plane. Previous studies concluded that the A-termination is preferred [25], and this structure is investigated here.

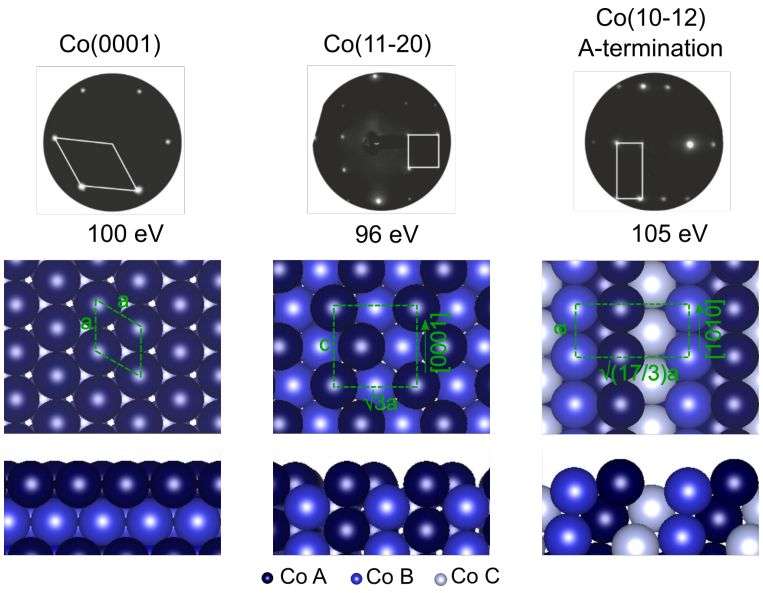

Fig. 1: Surface structure (top and side views) and LEED patterns of the Co(0001), Co(11–20), and the Co(10–12) surfaces. The surface unit cells and lattice parameters are indicated. For the corrugated surfaces the labels A, B and C are used to indicate the layer in which the cobalt atom is located.

Hydrogen adsorption and desorption: Temperature programmed desorption was used to study the adsorption and desorption dynamics of H_2. Fig. 2 shows a series of H_2 desorption spectra after dosing the indicated quantity of H_2 to the three different samples held at 100 K during exposure to H_2.

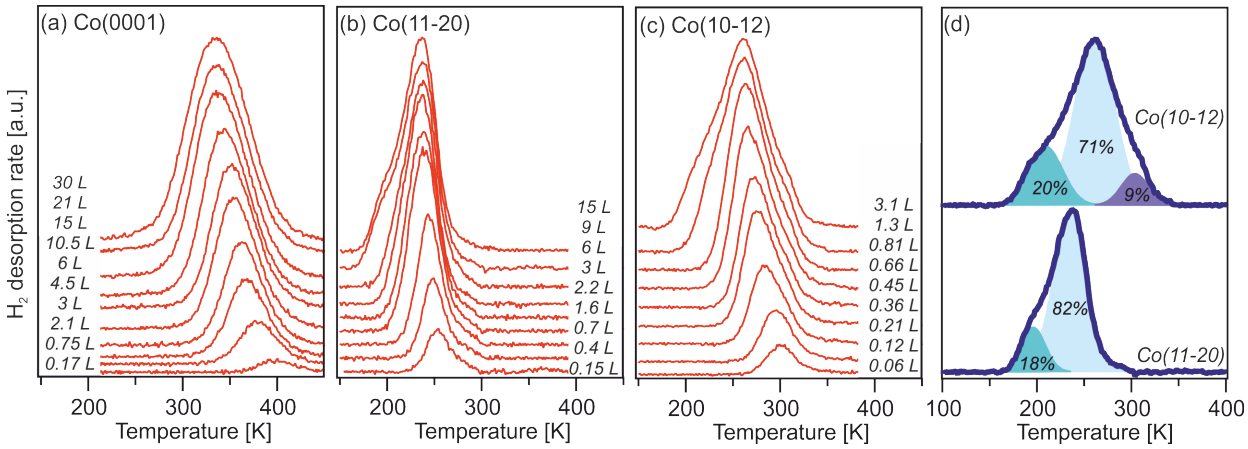

Fig. 2: H_2 desorption spectra after dosing H_2 at a sample temperature of 100 K on the three different surfaces. A heating rate of 2 Ks^{-1} was used in all cases.

In line with previous reports [5–7], the H_2 desorption spectra for the flat surface, shown in Fig. 2(a), consist of a single H_2 desorption peak. The downward shift of the peak maximum with increasing hydrogen coverage, from 400 K for the lowest coverage to 330 K for the highest coverage, is typical for a second order desorption process such as expected for the recombinative desorption of two H_{ad} to form H_2. The previously established H_{ad} saturation coverage of 0.5 ML (9.15 H per nm^2) is reached after a dose of 20-30 L.

Desorption from the more open Co(11-20) surface, shown in Fig. 2(b), occurs at a much lower temperature. The desorption peak maximum shows a modest shift as a function of surface coverage, from 254 K for low coverage to 235 K for high coverage. This high temperature desorption peak saturates after dosing 6 L, whereas a small shoulder develops for higher exposures which reaches a saturation point after a dose of 9 L. As described in the experimental section, the system pressure rise caused by desorption of 0.5 ML H_{ad} from the Co(0001) sample was used as a reference to quantify the hydrogen coverage on the Co(11-20) surface. This approach yields a hydrogen coverage of 6.8 hydrogen atoms per nm^2 for the highest coverage observed in our experiment. Deconvolution of the spectrum using two peaks with a gaussian shape, shown in Fig. 2(d), reveals that the main peak, centred at 240 K, accounts for ~5.6 hydrogens per nm^2, whereas the shoulder centred at 195 K accounts for ~1.2 hydrogens per nm^2. Since the density of row atoms is 11.3 per nm^2 on Co(11-20), this implies that the 240 K desorption peak corresponds to 1 H_{ad} per two zigzag row atoms.

For the Co(10-12) surface the desorption of hydrogen occurs between 200-320 K. A small high temperature desorption peak centred around 300 K saturates after a small dose of 0.12 L already. The main desorption peak saturates after a dose of around 1 L, with the peak maximum at the saturation point located at 260 K. A low temperature shoulder develops for

exposures >1 L, reaching a saturation point around 3 L (spectra for higher doses not shown here). Quantitative analysis shows a coverage of 9.3 hydrogen atoms per nm^2 at this point, that is, 1.4 hydrogen atoms per surface unit cell [see Fig. 1(c)]. Fig. 2(d) shows that the spectrum after dosing 3 L can be deconvoluted into three components, where the high temperature shoulder accounts for ~9% of the total. The main peak accounts for 71% of the total whereas the low temperature shoulder accounts for 20% of the total. Thus, after saturation of the main desorption peak centred at 260 K, the surface hydrogen concentration equals ~1 H_{ad} per surface unit cell.

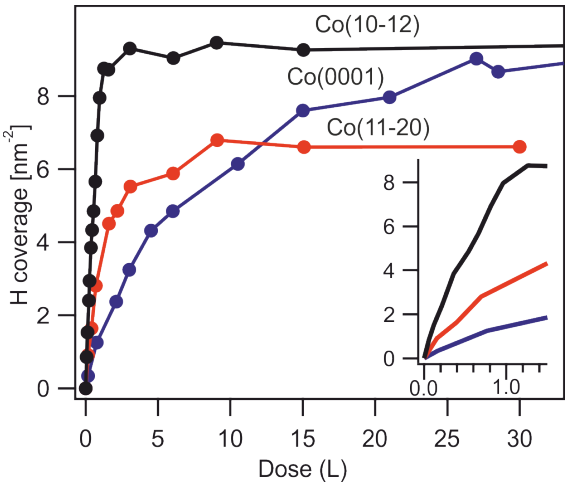

Fig. 3: Hydrogen coverage as a function of dose for the three different Co surfaces held at 100 K.

Fig. 3 shows the hydrogen coverage as a function of H_2 dose for the three surfaces investigated in this work. This graph clearly illustrates that the dissociative sticking coefficient of H_2 strongly depends on the structure of the surface. The Co(10-12) surface is the most reactive, requiring only a dose of ~1 L to reach saturation. Although the Co(11-20) surface also exposes a large concentration of surface atoms with a low coordination number, the initial sticking coefficient for H_2 on this surface is ~32% of that of the Co(10-12) surface. The initial sticking coefficient is lowest on the Co (0001), around only 10% of the value for the Co(10-12) surface. Table 1 contains a summary of the experimental findings. It should be

noted that absolute sticking coefficients can only be determined using special equipment. The values reported are therefore relative to the Co(10-12) surface for which the dissociative sticking coefficient was highest.

Table 1: Relative sticking coefficient and the saturation coverage observed in our experiments for the three surfaces studied. The activation energy for desorption was derived using a second order Redhead approximation assuming a pre-factor of 1×10^{13} ML^{-1} s^{-1}.

Facet	Relative sticking coefficient	UHV saturation coverage [H_{ad}/nm^2]	Activation energy for desorption [kJ mol^{-1}]
Co(0001)	0.1	9.2	92±7
Co(11-20)	0.32	6.6	61±4
Co(10-12)	1	9.3	72±5

Computational Results

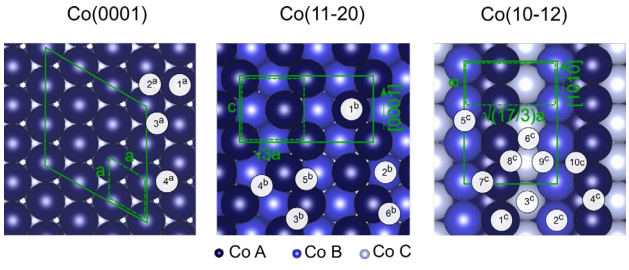

Fig. 4: Top views of the Co(0001), Co(11–20), and the Co(10–12) surface models together with the adsorption sites considered for each surface slab. The unit cell of each surface, and the surface unit cells used for the calculations, are indicated with dotted and solid green lines, respectively. The sites considered for the three surfaces; four sites for Co(0001): 1^a=t, 2^a=b, 3^a=h_{FCC}, 4^a=h_{HCP}; six sites for

Co(11-20): 1^b=t_A, 2^b=t_B, 3^b=b_A, 4^b=b_B, 5^b=$3h_{AAB}$, 6^b=$3h_{ABB}$; ten sites for Co(10-12): 1^c=t_A, 2^c=t_B, 3^c=t_C, 4^c=b_A, 5^c=b_B, 6^c=b_C, 7^c=b_{AB}, 8^c=$3h_{AAC}$, 9^c=$3h_{BBC}$, 10^c=4fH. The letters t, b and h stand for top, bridge and hollow adsorption sites.

DFT calculations were performed to further investigate how the adsorption strength of hydrogen depends on the structure of the cobalt surface. Fig. 4 illustrates the surface unit cells of the model Co surfaces used for the DFT calculations, where the different high symmetry sites explored for hydrogen adsorption are labelled. The Co(0001) surface exhibits four different sites: i.e. top (t), bridge (b), fcc-hollow (h_{FCC}), and hcp-hollow (h_{HCP}) sites [Fig. 4(a)]. The Co(11–20) facet exposes a corrugated surface with zigzag rows of Co atoms along the [0001] direction [Fig. 1(b)]. The atoms in the outermost rows have a coordination number of 7 and are referred to as the A-layer. The surface atoms between the rows have a coordination number of 11 and are referred to as the B-layer. This surface contains a larger number of high symmetry sites, namely two types of top sites, (t_A, t_B), two types of bridge sites (b_A, b_B), and two different types of 3-fold-hollow ($3h_{AAB}$, $3h_{ABB}$) sites, as indicated in Fig. 4(b). The Co(10–12) surface consist of three different layers and exhibits an even larger number of possible adsorption sites, namely; three top sites, (t_A, t_B, t_C), four bridge sites, (b_A, b_B, b_C, b_{AB}), two 3-fold hollow ($3h_{AAC}$, $3h_{BBC}$) sites, and one 4-fold hollow (4fH) sites, as indicated in Fig. 4(c). It exposes atoms in two layers below the top rows and may be regarded as a stepped surface.

H adsorption at low coverages: The energetic and structural parameters for adsorption of a single hydrogen atom per unit cell on various high symmetry adsorption sites of the p(3×3), p(2×1), and p(3×1) surface unit cells of the Co(0001), Co(11–20), and Co(10–12) surfaces, respectively, are listed in Table 2. It is worth mentioning that the calculated adsorption energies for “unstable” sites are obtained by fixing the position of the H atom along the x-

and y-axes, i.e., in the surface plane, and relaxing the distance along the z-axis. Otherwise, a complete relaxation of geometry results in moving the H atoms to nearby stable sites.

For the close-packed (0001) surface, the most favourable adsorption site for a single H atom in the p(3×3) unit cell is the h_{FCC} site, followed by a h_{HCP} site (Fig. 4), with the adsorption energies of –0.50 eV, and –0.47 eV, respectively (Table 2). This is in good agreement with previous DFT studies on the Co(0001) and Co(111) surfaces [5,9,18,19]. The presence of imaginary modes in the calculation of the vibrational modes show that bridge (B) and top (T) sites are not the local minima, and the energy values were obtained by fixing the x and y coordinate as discussed in the previous paragraph.

For the Co(11–20) facet, H adsorbs preferentially in the $3h_{AAB}$ site, where H binds to two A-row and one B-row atoms of the Co surface. The adsorption energy is –0.34 eV, only slightly larger than the H in the b_A site (–0.32 eV). This is, however, considerably lower compared to the adsorption energy found for H on the Co(0001) surface. Hence, this can explain the low H_2 desorption temperature of around 250 K obtained experimentally for this surface in comparison to 400 K for Co(0001).

For the Co(10–12) surface the calculations show that the 4fH site is the most favourable adsorption site, with an adsorption energy of –0.47 eV, almost the same as the most favourable site on the Co(0001) surface. The bridge site between two atoms in the B layer, (b_B), is the second-most favourable site followed by $3h_{AAC}$, and $3h_{BBC}$ sites, respectively. Hydrogen adsorption was not stable at the top and b_A sites, and the adsorbate moved to nearby stable sites during relaxation. This is corroborated with the presence of imaginary modes in the calculated vibrational modes presented in Table 2. The decrease in adsorption energy from going from Co(0001) to Co(10-12) to Co(11-20) is qualitatively in line with the

trend in the desorption temperatures observed in the low coverage TPD spectra (Fig. 2) for the three surfaces.

Table 2: Zero-point energy corrected adsorption energies (E_{ads}), differential Gibbs free energy of adsorption at 100 K and standard pressure, the nearest distance to the Co atoms (d_{Co-H}), and lists of the calculated vibrational frequencies (ν_i) of a hydrogen atom adsorbed at the various adsorption sites on the Co surfaces. Adsorption sites are illustrated in Fig. 4.

Facet/Slab	site	E_{ads}[eV]	ΔG_{ads} [eV]	d_{Co-H} [Å]	ν_i [cm^{-1}]
(0001)	t	0.06	0.13	1.51	1796, 369i, 369i
p(3×3)	b	–0.37	-0.31	1.67	1260, 1123, 496i
	h_{HCP}	–0.47	-0.41	1.74	1123, 823, 823
	h_{FCC}	**–0.50**	**-0.43**	**1.73**	**1133, 877, 877**
(11-20)	t_A	0.13	0.19	1.53	1782, 125i, 382i
p(2×1)	t_B	–0.25	-0.18	1.63	1371, 329i, 437i
	b_A	–0.32	-0.25	1.67	1344, 1055, 285
	b_B	–0.28	-0.22	1.79	980, 843, 624
	$3h_{AAB}$	**–0.34**	**-0.27**	**1.72**	**1147, 783, 495**
	$3h_{ABB}$	–0.26	-0.19	1.76	983, 875, 611
(10-12)	t_A	0.06	0.13	1.53	1739, 315i, 439
p(3×1)	t_B	0.03	0.09	1.52	1794, 110i, 384i
	t_C	–0.31	-0.25	1.63	1357, 198, 425i
	b_A	–0.29	-0.22	1.66	1253, 1073, 163i
	b_B	–0.38	-0.22	1.66	1294, 1138, 260
	b_C	–0.32	-0.25	1.77	960, 949, 652
	b_{AB}	–0.31	-0.25	1.65	1319, 1048, 93
	$3h_{AAC}$	–0.36	-0.30	1.72	1109, 888, 771
	$3h_{BBC}$	–0.35	-0.29	1.75	1107, 898, 641
	4fH	**–0.47**	**-0.40**	**1.89**	**791, 621, 561**

Coverage effect on H adsorption: The influence of coverage on the hydrogen adsorption strength was systematically investigated by adding hydrogen atoms to the unit cell and exploring various possible configurations to determine the one with the lowest total energy. Figs. 5(a)-(f) show two different coverages for the three surfaces to illustrate the occupation of different adsorption sites with increasing coverage. Either the differential adsorption energy or the differential Gibbs free energy of adsorption are commonly used to follow the build-up towards the saturation coverage on surfaces [40,41], as these values reflect the amount of energy gained when adding a new adsorbate to the existing coverage. Figs. 5(g) shows the calculated differential Gibbs free energies as a function of H coverage per nm^2 for all three Co surfaces. The saturation coverage is given by the point where the differential Gibbs free energy of adsorption becomes positive.

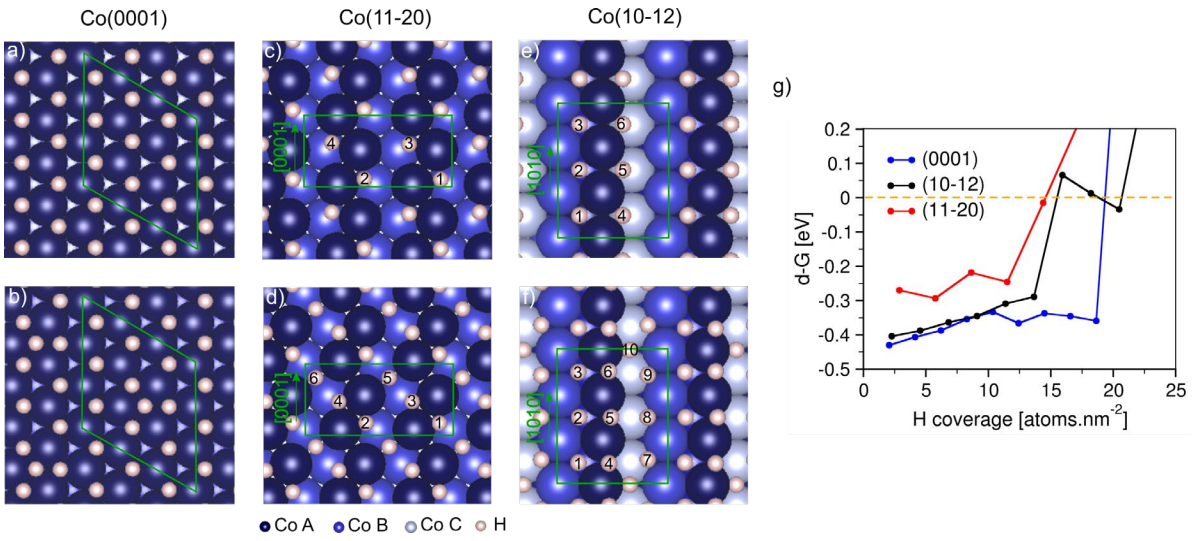

Fig. 5: Calculated hydrogen adsorption sites and energies as a function of coverage. (a-f) show the hydrogen adsorption sites for two different coverages for Co(0001), Co(11-20) and Co(10-12), with (c-f) showing the order in which the surface sites are filled following the lowest energy pathway. (g) shows the differential Gibbs free energy at 100K as a function of coverage for Co(0001), Co(10–12), and Co(11–20).

For Co(0001), the strongest adsorption site is the h_{FCC} site, and these sites are occupied exclusively during the process of covering the surface with hydrogen. The differential Gibbs

free energy of adsorption slightly decreases (becomes less negative) with increasing coverage, indicating that lateral interactions reduce the adsorption energy of hydrogen. The differential Gibbs free energy increases sharply when additional hydrogen is added after all h_{FCC} sites are filled. Fig. 5(a) shows a model of the adsorbate-covered surface at this point. When more hydrogen is added, the h_{HCP} sites start to be populated, as shown in Fig. 5(b). With all adjacent h_{FCC} sites filled already this is energetically unfavourable, and the differential Gibbs free energy becomes positive at this point. Since the energy differences between different configurations at a given coverage on Co(0001) were negligible we did not include the order in which the sites are filled in Fig. 5(a,b).

For the Co(11-20) surface we find that the second hydrogen added to the (2×1) unit cell preferentially occupies a $3h_{AAB}$ site located in a different row on the surface. The third and fourth hydrogen atoms adsorb with a slightly lower differential Gibbs free energy and occupy the next $3h_{AAB}$ sites along the A-row Co atoms denoted 3 and 4 in Fig. 5(c). However, these H-atoms shift to the adjacent $3h_{AAB}$ sites (denoted 3 and 4 in Fig. 5(d)) upon addition of the hydrogen atoms occupying positions denoted 5 and 6. This is due to the repulsive interactions caused by close proximity of H atoms in 3 and 4 to the newly adsorbed H in positions 5 and 6. Consequently, the added hydrogen not only adsorbs less strongly, but it also destabilizes the hydrogen atoms that are already present. This combined effect explains why adding a fifth hydrogen causes a step change in the differential Gibbs free energy, and a similarly large step change following the addition of a sixth hydrogen in the unit cell shifts the differential Gibbs free energy above zero [Fig. 5(g)].

For the Co(10–12), the most favourable adsorption site is the 4-fold hollow site, and up to three H atoms are accommodated on these sites in the (3×1) unit cell, as shown in Fig. 5(e). Although the bridge site between two atoms in the B-layer, b_B, is the second-most stable adsorption site for low coverage, we find that adsorption in these sites is disfavoured when

the adjacent 4-fold hollow sites are filled. Instead, the 3-fold-hollow sites ($3h_{BBC}$) denoted 4, 5, and 6 in Fig. 5(e) are occupied. When additional hydrogen atoms are added they occupy the 7, 8, and 9 positions on the surface. Filling of these sites leads to a destabilization of the hydrogens adsorbed in positions 4, 5 and 6, and, as a consequence, they slightly move toward the b_B sites, as shown in Fig. 5(f). At this point the coverage is already rather high, and the differential Gibbs free energy plot [Fig. 5(g)] shows an overall decrease in stability due to increasing coverage from 6H to 9H per (3×1) unit cell (from 13.4 to 20.1 H per nm^2). This may be attributed to lateral interactions between the hydrogen adsorbates. However, increasing the H coverage beyond 9 H (20.1 H per nm^2) is no longer energetically favourable as evident from the positive differential Gibbs free energy change.

Discussion

Since adsorbed hydrogen atoms are directly involved in the elementary reaction steps that affect the activity and the selectivity of the FTS reaction [42] it is worthwhile to explore the structure dependence of hydrogen adsorption in detail. The data shown here indicate that the influence of surface structure on the adsorption of hydrogen is surprisingly large, and both the adsorption kinetics, that is, the dissociative sticking probability, as well as the adsorption strength of adsorbed hydrogen atoms depend on the structure of the surface.

Hydrogen adsorption strength and H_2 desorption temperature

The TPD data shows that the hydrogen desorption temperature is a strong function of surface structure. This is in agreement with the DFT calculations, which show that the hydrogen adsorption strength is the highest for hydrogen adsorbed in the 3-fold hollow sites on Co(0001). By using a second-order Redhead method [43] with an assumed pre-exponential factor of 1×10^{13} $ML^{-1}s^{-1}$ we find an activation energy for H_2 desorption of 92 (±7) kJ mol^{-1}

(0.48 ± 0.04 eV/H_{ad}) in the low coverage regime (θ_H = 0.07 ML), close to the computed value and in line with earlier work [5]. On Co(10-12), H_{ad} instead prefers to adsorb in the 4-fold hollow site, but its bond strength is lower than that on the close-packed surface. A simple Redhead analysis of the main desorption peak yields a barrier of ~72(±5) kJ mol^{-1} (0.37 ± 0.03 eV/H_{ad}), somewhat lower than the computed adsorption energy of hydrogen on this surface. Hydrogen adsorbs weakest on the Co(11-20) surface. Although threefold hollow sites are available on this surface, the low H_2 desorption temperature, around 250 K, shows that the hydrogen adsorbs much weaker in these sites compared to the threefold sites on the Co(0001) surface. This is confirmed by the DFT calculations, which show a particularly low differential heat of adsorption on the Co(11-20) surface. In this case the Redhead approach for second order desorption yields a desorption barrier of around 61(±4) kJ mol^{-1} (0.316 ±0.02 eV/H_{ad}) for the main desorption peak, close to the value found in our computational study.

Hydrogen saturation coverage and the role of defect sites

The theory calculations shown in Fig. 5 indicate that it is energetically feasible to adsorb up to 1 ML of hydrogen on the Co(0001) surface. This coverage cannot be reached on a single crystal surface with low defect density, since the dissociative sticking coefficient drops to a very low value for θ_H>0.5 ML. In other words, the experimentally observed H_{ad} saturation coverage of 0.5 ML H_{ad} is limited by the difficulty to dissociate H_2 on a H-covered surface [11]. On the close-packed surface this (kinetic) limitation can be circumvented by introducing defects in modest concentrations, either by ion sputtering [5] or by using nm-sized Co islands where the edges act as catalysts for H_2 dissociation [15]. These defects act as a catalyst for H_2 dissociation [13] and on the sputter-damaged Co(0001) their presence has two effects: (i) the clean surface becomes more reactive, as the initial sticking coefficient for dissociative H_2 adsorption increases by one or two orders of magnitude. (ii) The sticking coefficient remains

high even when the H_{ad} coverage reaches 0.5 ML, and as a consequence the energetically favourable saturation coverage of ~1 ML can be reached [5,15]. For sputter-damaged Co(0001) (as well as for Co nano-islands) the defect sites, which efficiently catalyse H_2 dissociation, are located next to extended close-packed terraces where the dissociation products, H_{ad}, binds more strongly than on the defect sites themselves (as can be seen from the values in Table 2). Since the mobility of adsorbed hydrogen atoms on a metal surface is very high the energetically most favourable site occupation will be established at any practical temperature. Thus, the higher stability of H_{ad} on terrace sites drives diffusion of H_{ad} away from the defects, the active site for H_2 dissociation. This prevents poisoning of the active sites for H_2 dissociation so that H_2 dissociation can still take place even when the global coverage of H_{ad} exceeds 0.5 ML. In this way the energetically feasible coverage of 1 ML can be obtained experimentally.

The high initial sticking coefficient for dissociative H_2 adsorption on the corrugated Co surfaces confirms that undercoordinated surface atoms strongly promote H_2 dissociation. But the saturation coverage that can be reached on both corrugated surfaces is surprisingly low, much lower than the maximum coverage that would be energetically favourable. This shows that H_2 dissociation becomes poisoned by H_{ad} despite the high concentration of undercoordinated surface atoms on both surfaces studied.

The difference in adsorption energies of hydrogen atoms at different surface sites is key to understand why poisoning by H_{ad} occurs on Co(10-12) and Co(11-20) but not on defective Co(0001). By looking in detail into the structure of our surfaces we can understand why H_{ad} poisons dissociative H_2 adsorption on the corrugated surfaces but not on the defect-rich Co(0001) surface. On the Co(11-20) surface the most favourable adsorption site for H_{ad} is the threefold hollow site, where the hydrogen atom interacts with two 7-coordinated atoms in the outer row and one 11-coordinated atom in the second layer. The experimentally found

saturation coverage corresponds roughly to one hydrogen atoms per two row atoms, so at this point all row atoms are coordinated to one hydrogen atom. For Co(10-12) the most stable site is the 4-fold hollow site which are all occupied at the experimentally found saturation coverage. At this point all surface atoms with low coordination number coordinate to two hydrogen atoms. On the flat surface it was found that H_2 dissociation occurs on top sites [17] and it is reasonable to assume that the top sites of undercoordinated surface atoms are the active sites for H_2 dissociation on the corrugated surfaces. For both Co(11-20) and Co(10-12) hydrogen atoms prefer to reside close to the active site H_2 dissociation and in this way block these sites for a subsequent dissociation event. This is fundamentally different to the defective Co(0001) surface, where the presence of threefold sites on the terraces offer a more attractive place for hydrogen atoms to adsorb after dissociation on a defect site. As a consequence, defect sites remain available to catalyse H_2 dissociation up to a high hydrogen coverage.

Relevance for Fischer-Tropsch synthesis

Adsorbed hydrogen atoms are involved in many of the elementary reaction steps in Fischer-Tropsch synthesis. Steady state isotope kinetic analysis (SSITKA) experiments indicate that the hydrogen coverage under FTS conditions is low [44]: even for hydrogen-rich synthesis gas with $H_2/CO = 10$ the atomic hydrogen coverage was estimated to be in the order of 0.1-0.2 ML (1.5-3 H per nm^2 [45]), well below the experimentally found maximum coverage on any of the surfaces studied here. For the present study this implies that the results in the low coverage regime are most relevant for FTS catalysis.

A prominent finding of our study is the importance of undercoordinated surface atoms. They efficiently catalyse dissociative H_2 adsorption, but at the same time the dissociation products, surface hydrogen atoms, bind less strongly to undercoordinated sites. Instead, the threefold

hollow sites on the close-packed terrace are the preferred sites. Cobalt nanoparticles in a Co-based cobalt catalyst typically adopt the fcc bulk structure. The surface of such a particle is dominated by (111) and (100) facets with nm dimensions, terminated by step sites [2]. Translating the findings reported here to the morphology of nm-sized cobalt particles we propose that step sites are the primary source of hydrogen atoms during FT synthesis. H_2 dissociation occurs with high efficiency at step edges. Driven by the higher stability of hydrogen on terrace sites, the H_{ad} product quickly diffuses to an adjacent terrace where it can react in one of the many hydrogenation reactions required to transform CO into a long chain hydrocarbon product.

Conclusions

The present study shows that the interaction of H_2 with cobalt strongly depends on the exact structure of the surface. By combining the findings of experiments on a single crystal surface with insights obtained from theoretical calculations, we were able to show that the dissociative adsorption of H_2 is strongly enhanced by undercoordinated surface atoms. Furthermore, we found that H_{ad} is most strongly adsorbed in 3-fold hollow sites on the close-packed (0001) surface while the adsorption strength of hydrogen atoms on sites exposed on the more open (10-12) and 11-20) surfaces is significantly lower. For FTS catalysis we propose that dissociative adsorption of H_2 occurs primarily at step edges and kinks. The higher stability of hydrogen on terrace sites drives diffusion of the H_{ad} product away from steps onto the adjacent terraces.

Literature

[1] J. van de Loosdrecht, F.G. Botes, I.M. Ciobica, A. Ferreira, P. Gibson, D.J. Moodley, A.M. Saib, J.L. Visagie, C.J. Weststrate, J.W. Niemantsverdriet, in: J. Reedijk, K. Poeppelmeier (Eds.), Compr. Inorg. Chem. II, 2nd ed., Elsevier Ltd., 2013, pp. 525–557.

[2] P. van Helden, I.M. Ciobîcă, R.L.J. Coetzer, Catal. Today 261 (2016) 48–59.

[3] J.X. Liu, H.Y. Su, D.P. Sun, B.Y. Zhang, W.X. Li, J. Am. Chem. Soc. 135 (2013) 16284–16287.

[4] Q. Chen, I.H. Svenum, Y. Qi, L. Gavrilovic, D. Chen, A. Holmen, E.A. Blekkan, Phys. Chem. Chem. Phys. 19 (2017) 12246–12254.

[5] P. van Helden, J.-A. van den Berg, C.J. Weststrate, ACS Catal. 2 (2012) 1097–1107.

[6] K.M.E. Habermehl-Ćwirzeń, K. Kauraala, J. Lahtinen, Phys. Scr. T108 (2004) 28–32.

[7] Z. Huesges, K. Christmann, Zeitschrift Fur Phys. Chemie 227 (2013) 881–899.

[8] M.E. Bridge, C.M. Comrie, R.M. Lambert, J. Catal. 58 (1979) 28–33.

[9] D. Klinke, L. Broadbelt, Surf. Sci. 429 (1999) 169–177.

[10] A. Tuxen, S. Carenco, M. Chintapalli, C.H. Chuang, C. Escudero, E. Pach, P. Jiang, F. Borondics, B. Beberwyck, A.P. Alivisatos, G. Thornton, W.F. Pong, J. Guo, R. Perez, F. Besenbacher, M. Salmeron, J. Am. Chem. Soc. 135 (2013) 2273–2278.

[11] M. Sicot, O. Kurnosikov, H.J.M. Swagten, B. Koopmans, Surf. Sci. 602 (2008) 3667–3673.

[12] K. Christmann, Surf. Sci. Rep. 9 (1988) 1–163.

[13] R. van Lent, S. V. Auras, K. Cao, A.J. Walsh, M.A. Gleeson, L.B.F. Juurlink, Science

363 (2019) 155–157.

[14] E.A. Lewis, D. Le, A.D. Jewell, C.J. Murphy, T.S. Rahman, E.C.H. Sykes, ACS Nano 7 (2013) 4384–4392.

[15] E.A. Lewis, M.D. Marcinkowski, C.J. Murphy, M.L. Liriano, E.C.H. Sykes, J. Phys. Chem. Lett. 5 (2014) 3380–3385.

[16] K.-H. Ernst, E. Schwarz, K. Christmann, J. Chem. Phys. 101 (1994) 5388.

[17] B. Jiang, X. Hu, S. Lin, D. Xie, H. Guo, Phys. Chem. Chem. Phys. 17 (2015) 23346–23355.

[18] P. Ferrin, S. Kandoi, A.U. Nilekar, M. Mavrikakis, Surf. Sci. 606 (2012) 679–689.

[19] M. Yu, L. Liu, Q. Wang, L. Jia, B. Hou, Y. Si, D. Li, Y. Zhao, Int. J. Hydrogen Energy (2018).

[20] J.P. Perdew, K. Burke, M. Ernzerhof, Phys. Rev. Lett. 77 (1996) 3865–3868.

[21] Q. Wang, R. Zhang, L. Jia, B. Hou, D. Li, B. Wang, Int. J. Hydrogen Energy 41 (2016) 23022–23032.

[22] K. García-Díez, J. Fernández-Fernández, J.A. Alonso, M.J. López, Phys. Chem. Chem. Phys. 20 (2018) 21163–21176.

[23] H.J. Venvik, C. Berg, A. Borg, Surf. Sci. 402–404 (1998) 57–61.

[24] M.D. Strømsheim, I.H. Svenum, M.H. Farstad, Z. Li, L. Gavrilovic, X. Guo, S. Lervold, A. Borg, H.J. Venvik, Catal. Today 299 (2018) 37–46.

[25] K.A. Prior, K. Schwaha, M.E. Bridge, R.M. Lambert, Chem. Phys. Lett. 65 (1979) 472–475.

[26] P.E. Blöchl, Phys. Rev. B 50 (1994) 17953–17979.

[27] G. Kresse, D. Joubert, Phys. Rev. B - Condens. Matter Mater. Phys. 59 (1999) 1758–1775.

[28] G. Kresse, J. Furthmüller, Comput. Mater. Sci. 6 (1996) 15–50.

[29] G. Kresse, J. Furthmüller, Phys. Rev. B - Condens. Matter Mater. Phys. 54 (1996) 11169–11186.

[30] J.P. Perdew, K. Burke, M. Ernzerhof, Phys. Rev. Lett. 77 (1996) 3865–3868.

[31] H.J. Monkhorst, J.D. Pack, Phys. Rev. B 13 (1976) 5188–5192.

[32] M. Methfessel, A.T. Paxton, Phys. Rev. B 40 (1989) 3616–3621.

[33] A. Taylor, R.W. Floyd, Acta Crystallogr. 3 (1950) 285–289.

[34] D.R. Lide, H. V. Kehiaian, Handbook of Thermophysical and Thermochemical Data, 1st ed., CRC Press, Boca Raton, FL, 1994.

[35] K.P. Huber, G. Herzberg, Molecular Spectra and Molecular Structure 4: Constants of Diatomic Molecules, Van Norstrand Reinhold. Co., New York, USA, 1979.

[36] L. Bengtsson, Phys. Rev. B - Condens. Matter Mater. Phys. 59 (1999) 12301–12304.

[37] Z. Wang, H.-F. Wang, P. Hu, Chem. Sci. 6 (2015) 5703–5711.

[38] A. Plauck, E.E. Stangland, J.A. Dumesic, M. Mavrikakis, Proc. Natl. Acad. Sci. U. S. A. 113 (2016) E1973-82.

[39] K. Momma, F. Izumi, J. Appl. Crystallogr. 44 (2011) 1272–1276.

[40] S. Gudmundsdóttir, E. Skúlason, K.-J. Weststrate, L. Juurlink, H. Jónsson, Phys. Chem. Chem. Phys. 15 (2013) 6323.

[41] G. Hu, Q. Tang, D. Jiang, Phys. Chem. Chem. Phys. 18 (2016) 23864–23871.

[42] C.J. Weststrate, J.W. Niemantsverdriet, Faraday Discuss. 197 (2016) 101–116.

[43] P.A. Redhead, Vacuum 12 (1962) 203–211.

[44] J.P. Den Breejen, P.B. Radstake, G.L. Bezemer, J.H. Bitter, V. Frøseth, A. Holmen, K.P. de Jong, J. Am. Chem. Soc. 131 (2009) 7197–7203.

[45] R.C. Reuel, C.H. Bartholomew, J. Catal. 85 (1984) 63–77.